© 2017. Published by The Company of Biologists Ltd | Journal of Cell Science (2017) 130, 232-242 doi:10.1242/jcs.188151

SPECIAL ISSUE: 3D CELL BIOLOGY

RESEARCH ARTICLE

Ultrasound patterning technologies for studying vascular morphogenesis in 3D

Eric S. Comeau[1], Denise C. Hocking[1,2] and Diane Dalecki[1,*]

ABSTRACT

Investigations in this report demonstrate the versatility of ultrasound-based patterning and imaging technologies for studying determinants of vascular morphogenesis in 3D environments. Forces associated with ultrasound standing wave fields (USWFs) were employed to non-invasively and volumetrically pattern endothelial cells within 3D collagen hydrogels. Patterned hydrogels were composed of parallel bands of endothelial cells located at nodal regions of the USWF and spaced at intervals equal to one half wavelength of the incident sound field. Acoustic parameters were adjusted to vary the spatial dimensions of the endothelial bands, and effects on microvessel morphogenesis were analyzed. High-frequency ultrasound imaging techniques were used to image and quantify the spacing, width and density of initial planar cell bands. Analysis of resultant microvessel networks showed that vessel width, orientation, density and branching activity were strongly influenced by the initial 3D organization of planar bands and, hence, could be controlled by acoustic parameters used for patterning. In summary, integration of USWF-patterning and high-frequency ultrasound imaging tools enabled fabrication of vascular constructs with defined microvessel size and orientation, providing insight into how spatial cues in 3D influence vascular morphogenesis.

KEY WORDS: Ultrasound, Microvessels, Endothelial cell, Tissue engineering

INTRODUCTION

A major obstacle currently facing tissue engineering and regenerative medicine is the need for rapid and effective tissue vascularization strategies both during the fabrication of engineered tissues *in vitro* and upon construct implantation *in vivo*. Engineered three-dimensional (3D) microvascular networks are also expected to find widespread clinical use as a treatment to reverse tissue ischemia caused by disease or injury (Hitchcock and Niklason, 2008). In addition, there is a broad need for a variety of vascularized 3D models of physiological systems that can better predict efficacy, safety, bioavailability and toxicology outcomes for candidate therapeutics (Lin and Chang, 2008). To date, technologies that have the capacity to produce functional, small-caliber vascular networks within 3D tissue constructs are limited in number and remain in early stages of development (Bae et al., 2012). Identifying microenvironmental factors that influence blood vessel formation in 3D will expand our understanding of the mechanisms that control vascular morphogenesis and, in turn, provide new directions for advancing tissue vascularization strategies and microphysiological systems research. The present study utilizes an ultrasound-based system to volumetrically manipulate the spatial organization of endothelial cells in 3D in order to determine how geometric cues influence microvascular morphogenesis.

Ultrasound technologies offer new, non-invasive approaches to affect the 3D environment of cells (Dalecki and Hocking, 2015; Dalecki et al., 2016). One such technology employs the forces associated with a particular type of sound field, termed an ultrasound standing wave field (USWF), to rapidly direct the spatial organization of cells in hydrogels volumetrically and non-invasively (Dalecki and Hocking, 2015; Dalecki et al., 2016). USWFs are produced by the interference of two or more ultrasound fields. As one example, an USWF generated between an incident sound source and a reflector is characterized by regions of minimum acoustic pressure (i.e. pressure nodes) and maximum acoustic pressure (i.e. pressure anti-nodes). The nodal planes are perpendicular to the direction of sound propagation and are spaced at intervals equal to one half the wavelength of the incident sound field. If a solution of cells or microparticles is placed in an USWF, the acoustic radiation forces (F_{rad}) associated with the USWF act on the cells or particles to drive them to the pressure node locations (Gol'dberg, 1971; Gor'kov, 1962; Gould and Coakley, 1974). The magnitude of F_{rad} is given as

$$F_{rad} = \left(\frac{-\pi P_o^2 V \beta_o}{2\lambda}\right) \times \phi \times \sin\left(\frac{4\pi z}{\lambda}\right), \quad (1)$$

where P_o is the peak pressure amplitude in the USWF, V is the volume of the cell, $\lambda=c/f$ is the wavelength of the incident sound field, c is the speed of sound, f is the acoustic frequency of the sound field, and z is the perpendicular distance between a cell and the closest planar node. The parameter Φ is defined as the acoustic contrast factor between the cell and its surrounding medium,

$$\phi = \frac{5\rho_p - 2\rho_o}{2\rho_p + \rho_o} - \frac{\beta_p}{\beta_o}, \quad (2)$$

where, ρ_p and β_p are the density and compressibility of the cell, and ρ_o and β_o are the density and compressibility of the surrounding medium. As seen from Eqn 1, the magnitude of the radiation force driving cells to nodal locations is linearly proportional to the acoustic frequency, and to the square of the pressure amplitude of the incident sound field. As such, through correct design of acoustic field parameters, USWFs can predictably pattern cells at defined spatial locations.

USWFs have been utilized to rapidly and volumetrically pattern cells within 3D hydrogels (Garvin et al., 2013, 2010). In this

[1]Department of Biomedical Engineering, Goergen Hall, P.O. Box 270168, University of Rochester, Rochester, NY 14627, USA. [2]Department of Pharmacology and Physiology, 601 Elmwood Avenue, Box 711, University of Rochester, Rochester, NY 14642, USA.

*Author for correspondence (dalecki@bme.rochester.edu)

D.C.H., 0000-0003-2337-0357; D.D., 0000-0001-7114-9732

Received 16 February 2016; Accepted 18 October 2016

Journal of Cell Science

Journal of Cell Science (2017) 130, 232-242 doi:10.1242/jcs.188151

technology, cells are typically suspended in soluble collagen or fibrinogen and exposed to an USWF to spatially localize cells into planar bands spaced at half-wavelength intervals (Garvin et al., 2010). USWF exposure of the cell suspension is performed during the collagen or fibrin polymerization process. The phase transition of liquid to solid during the ultrasound exposure enables the 3D spatial patterning of cells to be retained after the sound field is removed. Ultrasound-mediated patterning of cells in 3D hydrogels has been demonstrated for a variety of cell types, including fibroblasts (Garvin et al., 2010), human umbilical vein endothelial cells (HUVECs) (Garvin et al., 2011, 2013), lymphatic microvascular endothelial cells (Dalecki et al., 2015), embryonic stem cells (Bouyer et al., 2016), neural cells (Bazou et al., 2005) and hepatocarcinoma cells (Liu et al., 2007). Importantly, USWF-patterning of cells has been shown to enhance cell function and promote cell-mediated extracellular matrix reorganization, without adversely affecting cell viability (Garvin et al., 2010).

This ultrasound-patterning technology offers a novel tool for scientists to study how a variety of different cell types respond in 3D environments. Ultrasound-mediated patterning of human endothelial cells into planar bands within collagen hydrogels leads to the emergence of capillary sprouts from the planar cell bands within 24 h and, within 10 days after USWF patterning, lumen-containing microvessel networks have self-assembled throughout the full 3D volume of the collagen hydrogel (Garvin et al., 2011, 2013). Our earlier studies suggested that the morphology of the resultant microvessel networks are influenced by the acoustic parameters of the USWF used to organize cells (Garvin et al., 2013). The ability of this USWF technology to pattern cells in 3D and, in turn, influence microvessel network formation offers a unique tool to study how 3D cellular organization influences the formation of distinct microvessel network morphologies.

In this paper, we report on new investigations designed to quantitatively characterize how acoustic exposure parameters influence USWF-driven cell patterning and, in turn, how initial 3D patterning of endothelial cells influences resultant microvessel network morphology. Ultrasound also offers unique tools to non-invasively and non-destructively image, and quantitatively characterize 3D tissue constructs during fabrication (Dalecki et al., 2016; Mercado et al., 2014, 2015). Thus, we also employed high-frequency ultrasound imaging to visualize and develop quantitative metrics in order to characterize the initial spatial organization of acoustically patterned cells throughout the depth of hydrogel constructs. Our results demonstrate the integrated effects of 3D spatial cues on vascular morphogenesis, wherein the spacing, width and density of the initial endothelial cell bands influenced microvessel width, orientation, density and branching activity. Similar morphological effects were obtained with endothelial cells derived from either small or large blood vessels, suggesting that endothelial cells from various tissue sources share common responses to spatial cues. Together, these results highlight the use of ultrasound-based technologies for 3D spatial patterning, quantitative imaging and the fabrication of 3D vascularized microphysiological systems.

RESULTS

3D cell patterning by using USWFs

USWFs were generated using the customized apparatus described in Materials and Methods and depicted in Fig. 1A. Unfocused piezoceramic transducers with resonant frequencies of 0.5, 1 or 2 MHz were used as acoustic sources. Characteristics of each transducer are provided in Table S1. The incident sound field was reflected with a steel plate, resulting in the generation an USWF throughout the volume of the sample. In this configuration, the pressure nodal planes are perpendicular to the direction of sound propagation and are spaced a distance equal to one half the wavelength of the incident sound. Thus, the distances between nodal planes for ultrasound propagation in water are 1500, 750 and 375 μm for 0.5, 1 and 2 MHz, respectively.

Mixtures of type I collagen (1 mg/ml final concentration) and human umbilical vein endothelial cells (HUVECs) were placed in modified cuvettes. Sample dimensions were 1×1×1 cm. Note that the −6 dB acoustic beam widths (Table S1) were equal to or greater than the width of the sample to enable cell patterning throughout the sample volume. Collagen–cell-solution mixtures were positioned in the sound field and exposed to an USWF. Acoustic radiation forces associated with the USWF organized cells into planar bands at nodal locations (depicted in Fig. 1B). Samples were exposed for a total of 15 min to allow the collagen to polymerize into a gel and, thus, trap the cells at nodal planes. Acoustic pressure amplitudes and cell-seeding concentrations investigated for each frequency are shown in Table S1. The acoustic radiation force acting on a cell is dependent upon both the acoustic frequency and the pressure amplitude (Eqn 1). Furthermore, the distance between node and anti-node increases with decreasing frequency. Thus, for comparison across acoustic frequencies, we chose pressure amplitudes, such that the acoustic radiation force gradient between node and anti-node remained constant across frequencies. Samples were exposed to continuous wave ultrasound for USWFs generated with 1- and 2-MHz sources. Pulsed exposures [pulse duration=70 μs, pulse repetition frequency (PRF)=3570 Hz] were employed for USWFs generated with the 0.5-MHz source in order to reduce acoustic cavitation in the water bath. In initial studies, ultrasound-induced heating was measured in cell–collagen samples and the maximum increase in temperature was 2°C. Therefore, water bath temperatures were adjusted slightly so that the final temperature in each sample at the end of the USWF exposure was 27°C for all exposure parameters tested. Sham-exposed samples (0 MPa) were subjected to identical procedures except the transducer was not activated. Following the 15-min exposure, samples were placed in an incubator set at 37°C and 5% CO_2.

High-frequency ultrasound imaging and quantification of 3D cell patterning

High-frequency ultrasound imaging was employed to visualize the initial 3D organization of cells produced by exposure to USWFs. Ultrasound imaging provides a depth of penetration unachievable with current light-microscopy imaging techniques, thereby enabling volumetric visualization of cell patterning throughout the hydrogel volume. Immediately after USWF exposure, backscatter (B-scan) images of cell-embedded collagen gels were generated using a 38-MHz transducer (Mercado et al., 2014, 2015). A schematic of the imaging protocol is depicted in Fig. 1C. Cells are the predominant scatterers within the cell-embedded collagen hydrogels (Mercado et al., 2014). Thus, in B-scan images of samples in these investigations, regions of increased brightness correspond to regions of higher cell concentration.

Representative B-scan images are shown in Fig. 2 for sham and USWF-patterned samples that had been prepared by using cell-seeding concentrations and acoustic parameters presented in Table S1. Image dimensions are 8.5 mm×6 mm. Cells were uniformly distributed within sham-exposed samples (Fig. 2A,E,I,M). In contrast, cell–collagen hydrogels patterned with 2-, 1- or 0.5-MHz

Journal of Cell Science (2017) 130, 232-242 doi:10.1242/jcs.188151

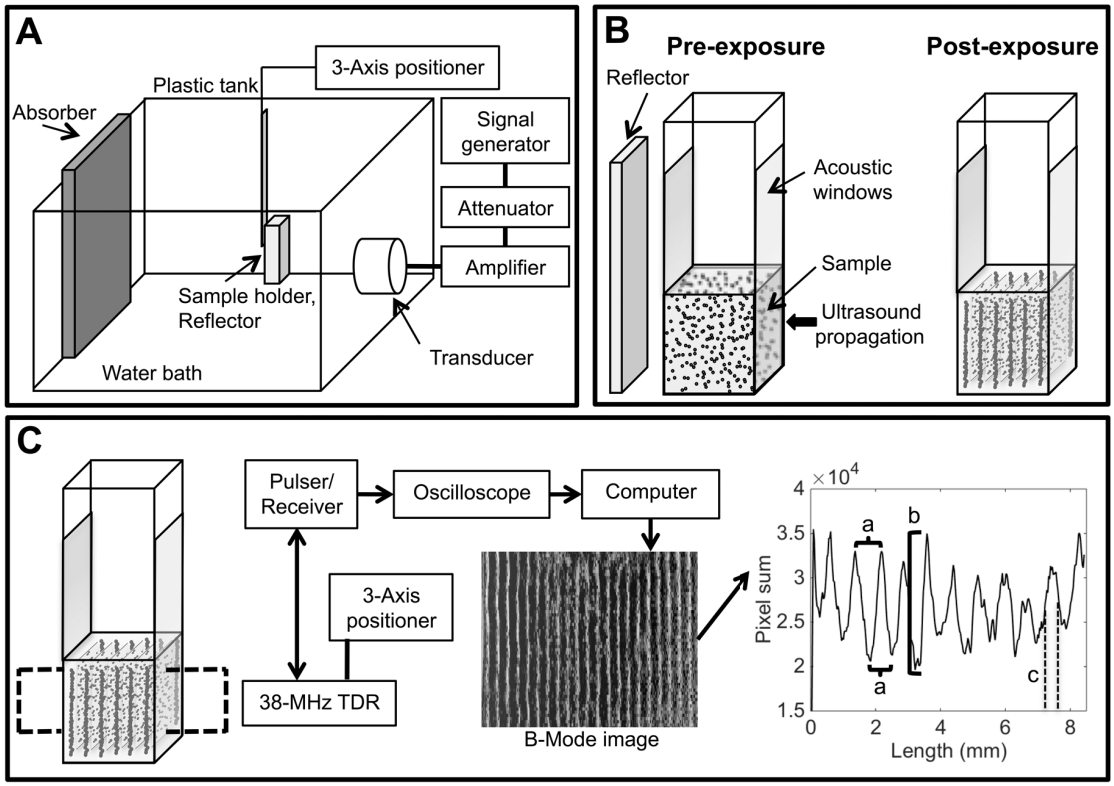

Fig. 1. Ultrasound systems used in order to pattern and image cells in collagen hydrogels. (A) Ultrasound sources were fixed in the side of a tank filled with degassed and deionized water. A signal generator, amplifier and attenuator drove the transducers to generate the ultrasound fields. Sample holders were located at the center of the ultrasound field using a three-axis positioner and a steel reflector was placed behind samples to generate an USWF through the sample volume. An acoustic absorber eliminated reflections from the back of the tank. (B) HUVEC (or HMVEC-D) and collagen samples were contained within modified plastic cuvettes. Parallel sides of cuvettes were replaced with acoustic windows to allow for almost lossless ultrasound propagation through the samples. The incident sound field was reflected by a steel plate resulting in an USWF. Acoustic radiation forces patterned cells into planar bands at nodal locations. (C) Samples were imaged by using high-frequency ultrasound to characterize cell patterning. A 38-MHz focused transducer (TDR) driven by a pulser-receiver was used to generate B-scans of the full thicknesses of HUVEC and collagen samples. Image processing of B-scans yielded three metrics to quantify cell patterning: (a) cell band spacing, (b) cell band density (i.e. NAC) and (c) cell band width.

USWFs showed increased brightness at nodal locations (Fig. 2). The distance between planar bands of cells increased with decreasing frequency (Fig. 2). For each frequency tested, the difference in brightness between nodal and anti-nodal regions increased as the pressure amplitude of the USWF increased (Fig. 2B-D,F-H,J-L), indicating increased local cell density at nodal regions in response to increasing pressure. At constant frequency and pressure amplitude, increasing the initial cell-seeding concentration also increased the cell density at nodal planes (Fig. 2N-P).

As demonstrated in Fig. 2, B-scan imaging provides qualitative visualization of cell patterning within collagen hydrogels. Further post-processing of B-scan images was then performed to provide quantitative metrics to characterize USWF-induced cell patterning. B-scan images were first compensated for axial beam patterns and attenuation as described in Materials and Methods. Gray scale values of each pixel within each column of an image were then summed and plotted as a function of the lateral distance of the image. Representative plots of these data are shown in Fig. S1. Three quantitative metrics to characterize the spatial patterning of cells were derived from graphs of USWF-patterned gels (depicted in Fig. 1C). First, the lateral distance between adjacent peaks or adjacent troughs was used to quantify the distance between nodal and anti-nodal regions, providing a metric of the distance between adjacent planar cell bands. Second, the full-width, half-maximum value of each peak was used to quantify the width of cell bands. Third, differences in the magnitudes of peaks and adjacent troughs were used to quantify the node-to-anti-node contrast (NAC), thereby providing a metric of relative differences in local cell concentrations between nodal and anti-nodal regions. Larger values of NAC indicate higher cell density within bands. Metrics were not derived for non-patterned, sham samples.

Fig. 3 provides mean values of each of these three quantitative metrics for all experimental conditions. The distance between adjacent planar cell bands increased with decreasing frequency (Fig. 3A). The mean (±s.e.m.) distance between cell bands patterned with 2-, 1- or 0.5-MHz USWFs were 389±4 µm, 727±1 µm or 1550 ±18 µm, respectively (Fig. 3A), consistent with predicted half-wavelength distances between nodal planes of the USWFs (Eqn 1). As also expected from Eqn 1, at a given frequency the distance between cell bands was not dependent on acoustic pressure amplitude (Fig. 3A), nor was cell band spacing affected by initial cell-seeding density (Fig. 3A,a-c).

For each frequency investigated, increasing pressure amplitude led to a significant decrease in the width of cell bands (Fig. 3B) and a corresponding increase in cell band density (i.e. NAC) (Fig. 3C). Taken together, these data indicate that increasing pressure amplitude serves to organize cells more densely into smaller volumes. When frequency and pressure amplitude were held constant at 0.5 MHz and 0.6 MPa, increasing the initial cell-seeding concentration resulted in decreased cell band width

Journal of Cell Science (2017) 130, 232-242 doi:10.1242/jcs.188151

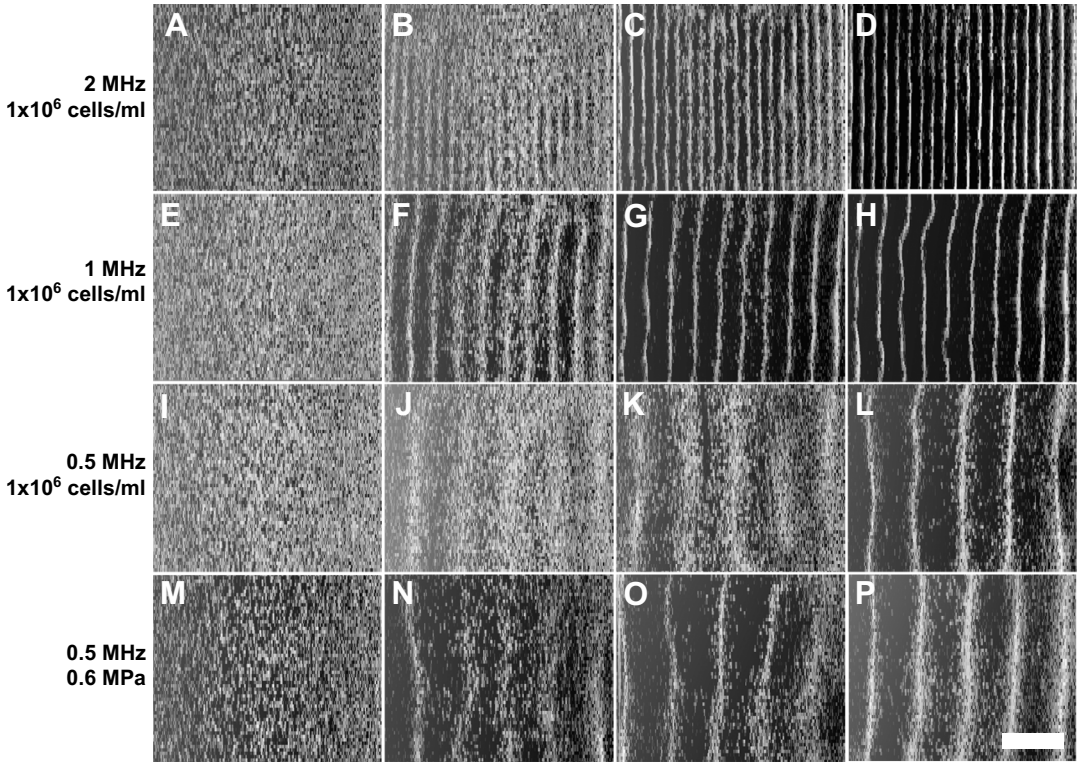

Fig. 2. Imaging USWF-induced 3D patterning of cells within thick collagen gels. High-frequency B-scan images were used to visualize differences in backscatter within collagen gels. Regions of higher backscatter represent higher local concentrations of cells. (A–D) Representative B-scans from studies at 2 MHz (1×10^6 cells/ml) for pressure amplitudes of 0, 0.05, 0.1 and 0.15 MPa are shown in panels A, B, C and D, respectively. (E–H) Representative B-scans from studies at 1 MHz (1×10^6 cells/ml) for pressure amplitudes of 0, 0.1, 0.2 and 0.3 MPa are shown in panels E, F, G and H, respectively. (I–L) Representative B-scans from studies at 0.5 MHz (1×10^6 cells/ml) for pressure amplitudes of 0, 0.2, 0.4 and 0.6 MPa are shown in panels I, J, K and L, respectively. (M–P) Representative B-scans from studies at 0.5 MHz (0.6 MPa) for cell-seeding concentrations of 0.25×10^6 cells/ml, 0.5×10^6 cells/ml and 1×10^6 cells/ml are shown in panels N, O and P, respectively; 1×10^6 cells/ml at 0 MPa data are shown in M. Sham samples (A, E, I, M) were not exposed (0 MPa) to USWFs. Images are representative of four to nine gels fabricated over at least three independent experiments for all acoustic and cell-seeding parameters tested. Scale bar: 2 mm.

(Fig. 3B,a-c) and increased cell band density (Fig. 3C,a-c), suggesting an increase in cell packing efficiency with higher cell concentrations. These data demonstrate that the spacing, width and density of 3D planar bands of cells, organized by using USWFs, can be reproducibly controlled through choice of acoustic frequency, pressure amplitude and cell-seeding density.

Influence of 3D cell patterning on microvessel morphology

The next experiments were conducted to determine how the initial geometric organization of endothelial cells influences the arrangement and morphology of resulting microvessel networks. HUVECs were acoustically patterned in collagen gels using the same frequencies and pressure amplitudes as analyzed above (Table S1 and Figs 2 and 3). The constructs were then cultured for 10 days, stained with MTT and imaged using light microscopy. Fig. 4 presents representative images of microvessel networks obtained in response to the various USWF exposure conditions and cell-seeding concentrations. Sham-exposed samples displayed some endothelial cell sprouting but minimal network formation (Fig. 4A,E,I,M). In contrast, USWF-patterned constructs contained extensive microvessel networks throughout the gel volume (Fig. 4B-D,F-H,J-L,N-P). Moreover, microvessel network morphology appeared to be dependent upon the acoustic exposure parameters used for initial USWF cell patterning, as well as the initial cell-seeding concentration (Fig. 4). Thus, to quantify differences in microvessel network morphology, microvessel width (Figs 5 and 6), alignment (Fig. 6) and density (Fig. 6) were measured as a function of USWF exposure parameters.

Effects of USWF parameters on the cross-sectional widths of resultant microvessels are presented as cumulative distribution graphs in Fig. 5. In all sham-exposed constructs, 95% of microvessels were ≤25 µm in cross-section (Fig. 5A-D) and there was no preferred direction of vessel alignment (data not shown). For constructs fabricated with 0.5-MHz USWFs (i.e. initial band spacing of ~1.5 mm), cross-sectional widths of self-assembled microvessels were also predominantly ≤25 µm for all pressure amplitudes tested (Fig. 5C). Small-caliber vessels also formed when HUVECs were patterned with 1- or 2-MHz USWFs and the lowest pressure amplitudes tested (Fig. 5A,B). Specifically, ~90% of vessels had cross-sectional widths ≤25 µm for constructs fabricated with 1-MHz USWFs at 0.1 MPa (Fig. 5B, solid squares), or 2-MHz USWFs at 0.05 MPa (Fig. 5A, solid squares). In comparison, larger microvessels formed in constructs fabricated with 1- and 2-MHz USWFs at higher pressure amplitudes (Fig. 5A,B). Interestingly, using 1-MHz USWFs with a pressure amplitude of 0.2 MPa produced constructs containing the largest diameter vessels where 83% of vessels had cross-sectional widths >50 µm, and 35% of vessels had cross-sectional widths >100 µm (Fig. 5B, open circles). Constructs fabricated with 1-MHz USWF and 0.3 MPa had a broad distribution of microvessel widths, where 50% of vessels were ≤25 µm and 40% of vessels were ≥50 µm (Fig. 5B, solid circles). In constructs fabricated with 2-MHz USWF and either 0.1 MPa or 0.15 MPa, ~65% of microvessels were ≥25 µm (Fig. 5A, solid and open circles, respectively). Using 0.5-MHz USWFs, larger microvessels were also fabricated by decreasing the initial cell-seeding concentration by half to 0.5×10^6 cells/ml (Fig. 5D).

Journal of Cell Science (2017) 130, 232-242 doi:10.1242/jcs.188151

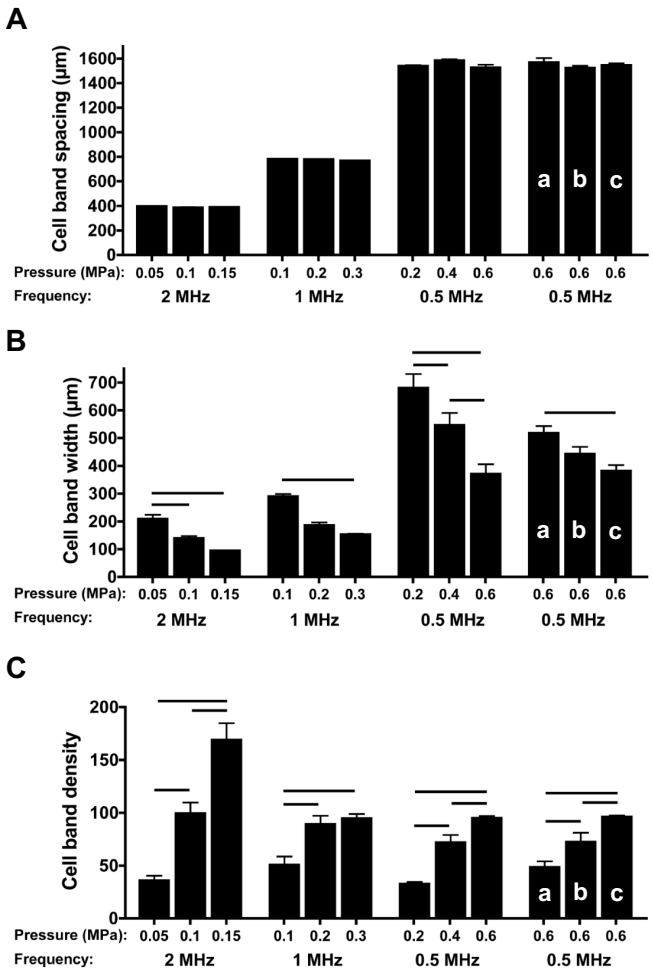

Fig. 3. Quantification of initial USWF-induced cell patterning in collagen hydrogels. (A–C) As described in Materials and Methods, data from post-processing of B-scan images (shown in Fig. S1) were then used to generate three metrics to quantify USWF-induced cell patterning: cell band spacing (A), cell band width (B) and NAC, i.e., cell band density (C). Cell patterning metrics were obtained for all experimental conditions shown in Fig. 2. Columns labeled a, b and c correspond to cell-seeding concentrations of 0.25×10^6 cells/ml, 0.5×10^6 cells/ml and 1×10^6 cells/ml, respectively. All other data were obtained by using cell-seeding concentrations of 1×10^6 cells/ml. Data represent mean± s.e.m. (n=4–9). At least three different gels, fabricated on separate days, were analyzed for each parameter examined. Horizontal bars represent statistical significance between groups (ANOVA, Bonferroni post hoc test, P<0.05).

Neither sham nor USWF-patterned constructs fabricated with 0.25×10^6 cells/ml remained viable over 10 days and, thus, were not analyzed further.

We next analyzed how microvessel cross-sectional width and alignment varied within nodal and anti-nodal regions of the original USWF. Only small diameter vessels (i.e. ≤25 μm) were present in anti-nodal regions regardless of the frequency or pressure amplitude used to initially pattern cells (Fig. 6A, hatched columns). Moreover, vessels in the anti-nodal regions were oriented primarily perpendicular to the initial cell band plane (Fig. 6B, hatched columns), indicating that small 'capillary-like' vessels formed between nodal planes. In comparison, when larger microvessels formed, they were confined primarily to the nodal regions and oriented parallel to the direction of initial cell bands. Specifically, for constructs patterned using 1- or 2-MHz USWFs, increasing pressure amplitude led to increasing microvessel widths within nodal regions (Fig. 6A), with vessels oriented parallel to the initially organized planar cell bands (Fig. 6B). Large-diameter microvessels were also observed in the nodal planes of constructs that had been patterned by using 0.5-MHz USWFs and a cell-seeding concentration of 0.5×10^6 cells/ml (Fig. 6A,B).

Vessel density was quantified from MTT-stained images as the percent area occupied by vessels. On average, vessel density of ultrasound-patterned constructs was greater than sham-exposed samples (50.1±4.4%, versus 20.4±5.3%, respectively) and was also dependent on the initial acoustic patterning parameters (Fig. 6C). For constructs patterned using 1- or 2-MHz USWFs, increasing pressure amplitude led to a reduction in overall microvessel density (Fig. 6C), consistent with the appearance of larger diameter vessels in the nodal regions (Figs 6A). Vessel density also decreased with decreased initial cell-seeding concentration. Taken together, these data demonstrate the integrated effects of 3D cell patterning parameters on microvessel network morphology, wherein the initial spacing, width and density of initial planar cell bands contributed to resultant microvessel diameter, alignment and density.

Microvessel constructs fabricated with HUVEC using 1-MHz USWFs at the three different pressure amplitudes were also analyzed histologically to analyze vessel lumen. Sections parallel to the direction of sound propagation (i.e. perpendicular to the initial planar cell bands) were obtained from the center of the gels and then stained with hematoxylin and eosin (Fig. 7A-E). Digital images of these sections were analyzed using ImageJ software to measure lumen area of vessels within the nodal regions (Fig. 7F). Constructs exposed to sham conditions formed few lumen-containing vessels (Fig. 7B); those that formed were predominantly 2000 μm^2 or smaller (Fig. 7F). In agreement with data shown in Fig. 6A, constructs fabricated by using 1-MHz USWFs and 0.1 MPa pressure amplitude produced predominantly small, lumen-containing vessels (Fig. 7A,C). Approximately 80% of vessels had lumen areas of ≤2000 μm^2 but a small percentage (7%) were >5001 μm^2 (Fig. 7F). Constructs fabricated with 1-MHz USWFs and 0.2 MPa pressure amplitude formed larger parallel vessels within the initial nodal planes (Fig. 7D). Almost 24% of these vessels had lumen areas ≥5001 μm^2 (Fig. 7F). Similarly, constructs fabricated with 1-MHz USWFs and 0.3 MPa pressure amplitude formed large vessels within areas of initial cell patterning (Fig. 7E), and 28% of these vessels had lumen areas of >5001 μm^2 (Fig. 7F).

Intercellular association of vascular endothelial (VE)-cadherin is required for vascular integrity *in vivo* (Corada et al., 1999). Thus, VE-cadherin staining was used to assess the quality of microvessels produced by patterning with 1-MHz USWFs (Fig. 7G). VE-cadherin-positive intercellular junctions were observed in microvessels fabricated at all three pressure amplitudes; Fig. 7G shows representative images of microvessels formed in response to patterning with 1 MHz, 0.3 MPa USWF. VE-cadherin staining appeared as sharp, continuous lines at cell–cell borders, demonstrating integrity of USWF-fabricated microvessels in both nodal and anti-nodal regions.

Functional differences in endothelial cells that reside at different vascular locations or within different tissues have been attributed to differences in endothelial cell size, shape and/or the complexity of cell-cell junctions (Staton et al., 2009). Thus, we next asked whether endothelial cells isolated from different vascular beds would respond similarly to USWF-mediated spatial patterning. To do so, adult dermal microvascular endothelial cells (HMVEC-D) were patterned using acoustic exposure parameters that gave rise to either small (<25 μm; 1 MHz, 0.1 MPa) or large (>50 μm; 1 MHz. 0.2 MPa) diameter HUVEC microvessel networks.

Journal of Cell Science (2017) 130, 232-242 doi:10.1242/jcs.188151

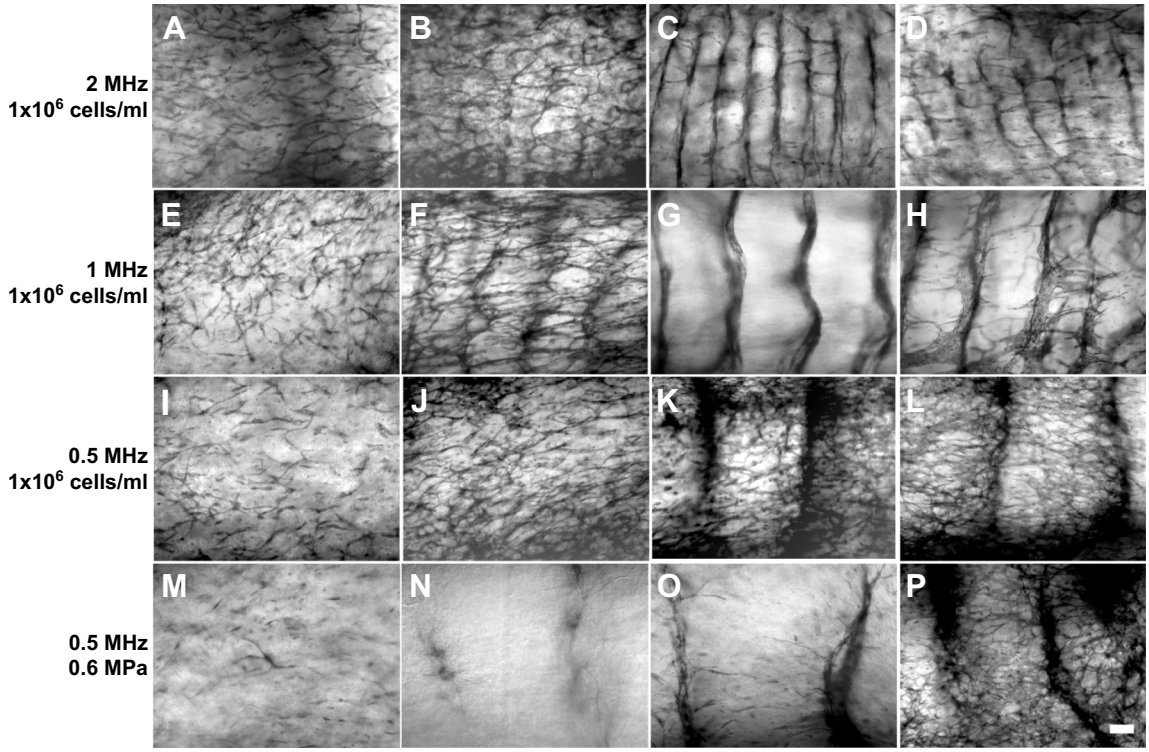

Fig. 4. Microvessel network formation in response to USWF-induced patterning. USWF-patterned and sham HUVEC samples were cultured for 10 days, then stained with MTT. (A–D) Representative images from studies at 2 MHz (1×10^6 cells/ml) for pressure amplitudes of 0, 0.05, 0.1 and 0.15 MPa are shown in panels A, B, C and D, respectively. (E–H) Representative images from studies at 1 MHz (1×10^6 cells/ml) for pressure amplitudes of 0, 0.1, 0.2 and 0.3 MPa are shown in panels E, F, G and H, respectively. (I–L) Representative images from studies at 0.5 MHz (1×10^6 cells/ml) for pressure amplitudes of 0, 0.2, 0.4 and 0.6 MPa are shown in panels I, J, K and L, respectively. (M–P) Representative images from studies at 0.5 MHz (0.6 MPa) for cell-seeding concentrations of 0.25×10^6 cells/ml, 0.5×10^6 cells/ml and 1×10^6 cells/ml are shown in panels N, O and P, respectively, and 1×10^6 cells/ml at 0 MPa data are shown in panel M. Scale bar: 250 µm. Images are representative of four to nine gels fabricated in at least three independent experiments.

Sham-exposed HMVEC-D did not form microvascular networks after 10 days in culture and exhibited limited viability (Fig. 8A). In contrast, HMVEC-D patterned with an USWF at 1 MHz and pressure amplitude of 0.1 MPa formed interconnected capillary-like networks (Fig. 8B). HMVEC-D patterned with an USWF of 1 MHz and pressure amplitude of 0.2 MPa (Fig. 8C) produced nodal vessels characterized by larger diameters (Fig. 8D), fewer branches (Fig. 8C) and lower overall density (Fig. 8E) than those formed in response to 0.1 MPa. Thus, morphological characteristics observed with 0.1 MPa-patterned versus 0.2 MPa-patterned HMVEC-D are similar to those observed when patterning HUVEC. That is, endothelial cells isolated originally from small vessels were induced

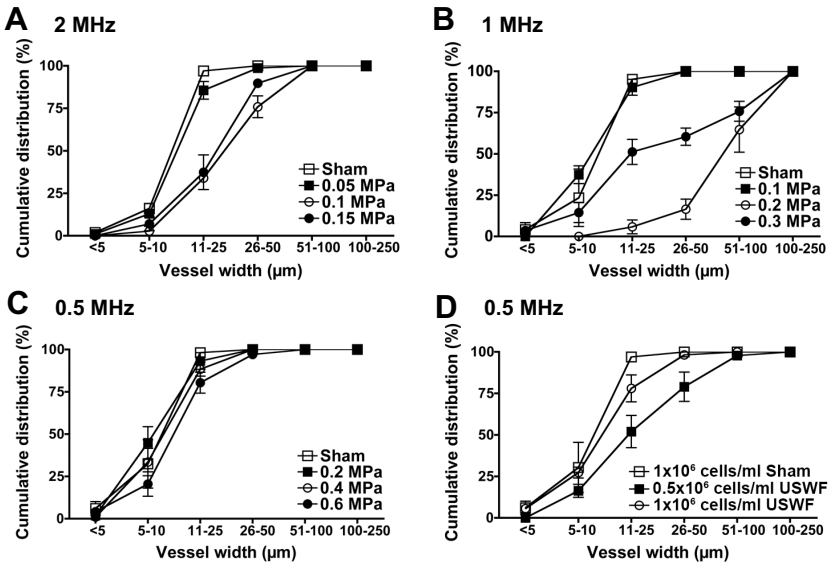

Fig. 5. Quantification of microvessel cross-sectional widths. (A–D) Light-microscopy images of MTT-stained HUVEC constructs were used to measure cross-sectional widths of microvessels. Cumulative distribution graphs were generated to depict the percentage of vessels with cross-sectional widths less than or equal to each bin size. Data from experiments at 2 MHz (1×10^6 cells/ml) and pressure amplitudes of 0, 0.05, 0.1 and 0.15 MPa (A). Data from experiments at 1 MHz (1×10^6 cells/ml) and pressure amplitudes of 0, 0.1, 0.2 and 0.3 MPa (B). Data from experiments at 0.5 MHz (1×10^6 cells/ml) and pressure amplitudes of 0, 0.2, 0.4 and 0.6 MPa (C). Data from experiments at 0.5 MHz (0.6 MPa) and cell-seeding concentrations of 0.5×10^6 cells/ml and 1×10^6 cells/ml (D). Measurements were collected from at least three images of four to nine samples per condition. Samples were fabricated in at least three independent experiments. Data are presented as mean±s.e.m. for the samples within each condition.

Journal of Cell Science (2017) 130, 232-242 doi:10.1242/jcs.188151

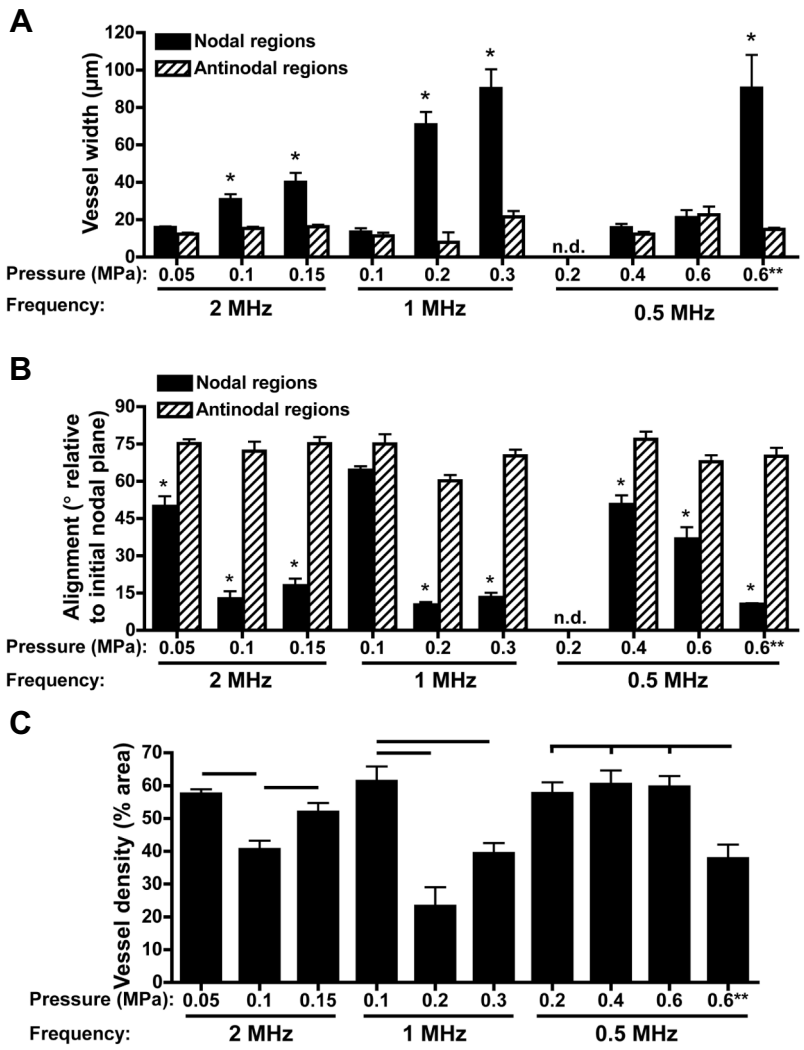

Fig. 6. Quantification of microvessel width and alignment within nodal and anti-nodal regions. (A–C) Light-microscopy images of MTT-stained HUVEC constructs were used to measure cross-sectional widths of microvessels (A), the direction of microvessel alignment relative to the initial nodal plane for both nodal (solid) and anti-nodal (hatched) regions (B) and microvessel density (C). Mean angle values of 0°–30° represent a preferred alignment in the initial direction of cell banding, 30°–60° represent no preferred alignment, 60°–90° represent a preferred alignment perpendicular to areas of initial cell banding. **, cell-seeding concentration of 0.5×10^6 cells/ml. No data (n.d.) were derived from samples fabricated with USWFs at 0.5 MHz and 0.2 MPa since nodal and anti-nodal regions were not distinguishable after 10 days of culture. Measurements were collected from at least three images of four to nine samples per condition. Samples were fabricated in at least three independent experiments. Data are presented as mean±s.e.m. (n=4–9). *Significantly different from other groups within the given frequency (ANOVA, P<0.05). In C, horizontal bars represent statistical significance between groups (ANOVA, Bonferroni post hoc test, P<0.05).

to form larger vessels *in vitro* and, vice versa, by altering spatial organization during patterning. These data provide initial evidence that endothelial cells from different tissue sources respond similarly to 3D spatial cues, and that the morphological features of engineered microvessel constructs can be controlled by using defined ultrasound-patterning parameters.

DISCUSSION

Ultrasound technologies are emerging as enabling tools for the fabrication of 3D tissue constructs for use in microphysiological systems research, tissue engineering and regenerative medicine therapies (Dalecki and Hocking, 2015; Dalecki et al., 2016). Ultrasound offers unique capabilities to interact with cells and/or extracellular matrix scaffolds through localized mechanical forces (Dalecki, 2004). Furthermore, ultrasound imaging provides non-invasive, non-destructive capabilities for visualizing 3D cell-based constructs (Dalecki and Hocking, 2015; Dalecki et al., 2016; Mercado et al., 2014, 2015). Investigations in this report demonstrate the versatility of ultrasound technologies for studying cells in 3D environments.

USWFs were employed as a non-invasive approach to rapidly and predictably pattern cells within 3D collagen hydrogels. In the single-source and reflector configuration used in these studies, forces associated with the USWF directed cells to nodal regions resulting in planar bands of cells throughout the volumes of collagen hydrogels. The frequency of the ultrasound field controlled the distance between cell bands, and the pressure amplitude controlled the local density of cells in the nodal regions relative to the anti-nodal regions. By using this USWF technology, more-complex patterning geometries might be achieved (such as columns or grids) when using more than one source and/or reflector.

High-frequency ultrasound imaging enabled visualization of USWF-induced cell patterning volumetrically through 3D collagen hydrogels. B-scan images were generated to visualize the influence of USWF exposure parameters on cell patterning. Note that the 38-MHz imaging source used in these studies does not have the spatial resolution to image individual cells. However, high-frequency ultrasound has the key advantage of providing backscatter images through the 1-cm depths of USWF-patterned collagen hydrogels. Three metrics were defined to quantify the initial USWF-induced arrangement of cells: cell band spacing, cell band width and cell band density. These metrics were capable of quantifying differences in cell patterning as a function of USWF exposure frequency and pressure amplitude, and initial cell-seeding density.

After 10 days of culture, the resultant morphology, size, alignment and density of microvessels within collagen gels were influenced by USWF exposure parameters used for initial 3D cell patterning. Constructs comprising extensive, small (≤25 μm) capillary-like vessels formed in response to USWF at the lowest pressure amplitudes tested for all frequencies. For these exposure

Journal of Cell Science (2017) 130, 232-242 doi:10.1242/jcs.188151

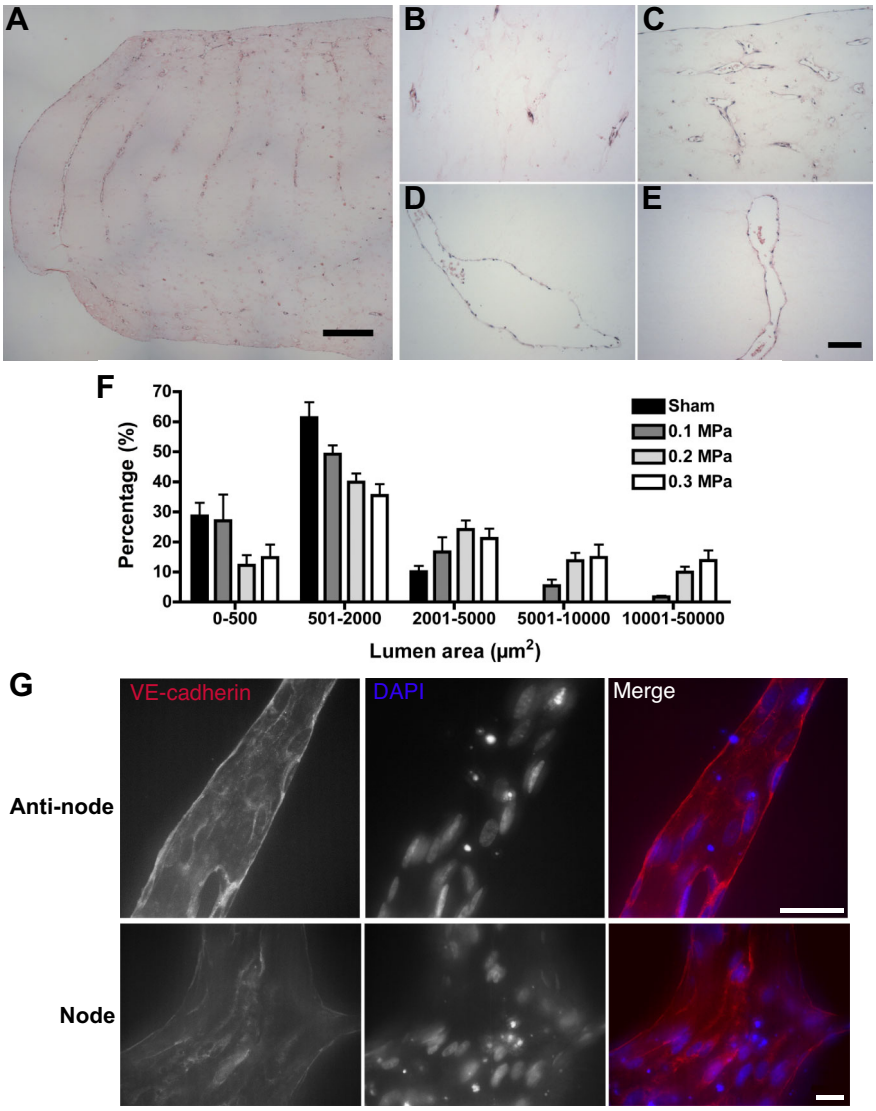

Fig. 7. Histological assessment of microvessel networks and quantification of microvessel lumen areas. (A–F) HUVEC microvessel constructs were fixed and sectioned through the center of the gel and stained with hematoxylin and eosin (A–E). Sections were imaged using light microscopy and lumen area was quantified using ImageJ software (F). Panel A is a representative image of a day-10 construct initially patterned by using 1-MHz USWF and 0.1 MPa pressure amplitude; scale bar: 500 µm. Higher magnification images of gels patterned using 1-MHz USWFs with 0 (B), 0.1 (C), 0.2 (D) and 0.3 (E) MPa pressure amplitudes are shown; scale bar: 100 µm. (F) Lumen areas were quantified as a function of pressure amplitude and displayed as a histogram. Data are presented as mean±s.e.m. of five sections with at least 25 non-overlapping images, obtained from each of two independent gels per condition. VE-cadherin was visualized in cell–cell junctions by using a rabbit polyclonal anti-VE-cadherin antibody (red). Cell nuclei were visualized with DAPI (blue). (G) Representative images obtained from both anti-nodal and nodal regions of day-10 constructs initially patterned using 1 MHz, 0.3 MPa. Scale bars: 20 µm.

conditions, cells initially aggregated loosely in nodal planes, as indicated by higher values of cell band width and lower values of cell band density (i.e. NAC). In these constructs, small microvessels formed in both nodal and anti-nodal regions. Notably, dense microvessel networks were present in anti-nodal regions even when the distance between initial cell bands was 1500 µm (i.e. 0.5 MHz, 0.2 MPa, Fig. 4B).

In general, larger microvessels formed when the pressure amplitude of the USWF increased. For each frequency tested, increasing pressure amplitude patterned cells more densely at nodal regions, as indicated by lower values of cell band width and higher values of cell band density (i.e. NAC). Vessels with widths >50 µm were only present within the nodal regions of the USWF, i.e. where cells were densely patterned initially. Furthermore, these large vessels in nodal regions were parallel to the direction of initial cell banding. Vessel widths reported in Figs 5 and 6 were obtained by using light microscopy to measure cross-sectional widths of vessels near the edges of collagen gels stained with MTT. However, histological sections revealed that, when viewed in the plane perpendicular to initial cell patterning, lumen areas of large vessels were typically ellipsoidal (Fig. 7). In constructs with the largest microvessels, lumen areas were >10,000 µm^2 (Fig. 7). Furthermore, vessels were evident throughout the full volume of the collagen hydrogels. The ability of acoustic patterning techniques to reproduce different structural features of native microvessel networks should allow for the fabrication of physiological models and pre-vascularized tissue constructs that can be more closely matched to the structure and function of target tissue.

VE-cadherin was localized within intercellular junctions of USWF-patterned microvessels formed at both nodal and anti-nodal planes (Fig. 7), providing evidence of microvessel integrity. Of note, and in contrast to previous reports (Blinder et al., 2015), USWF-fabricated microvessels self-assembled into robust, stable networks without the addition of stromal cells, indicating that particular spatial patterns of endothelial cells can provide information sufficient for microvessel formation in 3D. Similarly, acoustic patterning of endothelial cells that were derived from two different tissue sources resulted in morphologically similar microvessel networks. Specifically, endothelial cells that were derived from dermal capillaries of adults could be induced to form microvessels with a relatively large (~40 µm) or small (~10 µm) diameter. These studies provide evidence that 3D organizational cues are a principal, underlying component of vascular morphogenesis.

In summary, these investigations demonstrate the versatile capabilities of ultrasound technologies for studying cells in 3D

Journal of Cell Science (2017) 130, 232-242 doi:10.1242/jcs.188151

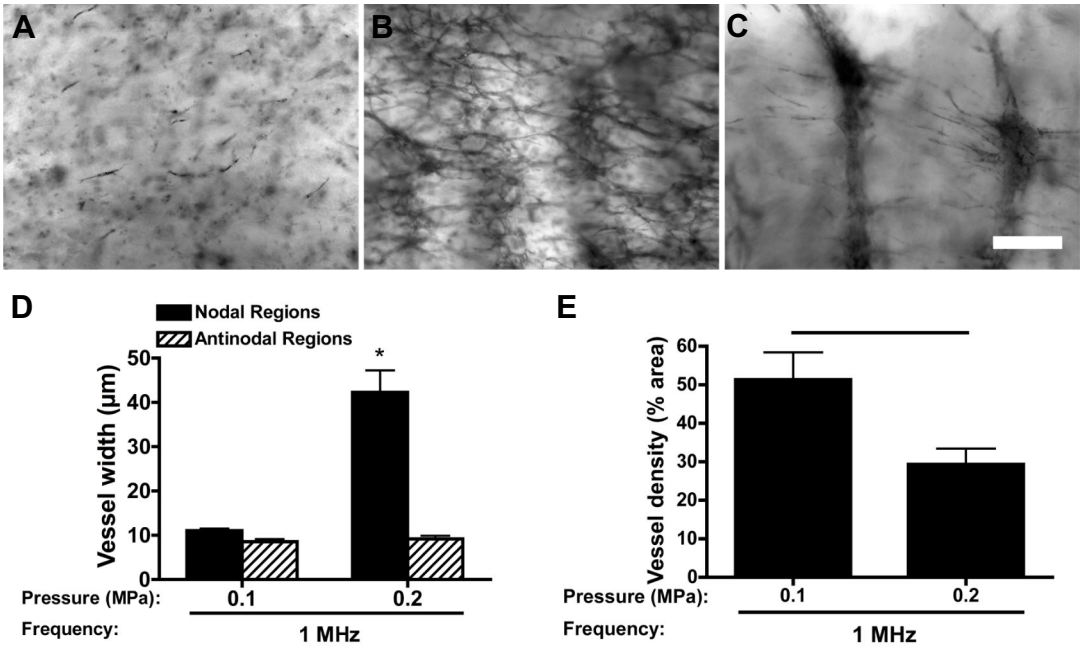

Fig. 8. Vessel network formation by microvascular endothelial cells in response to USWF patterning. (A–C) HMVEC-D (1×10^6 cells/ml) were suspended in solutions of type I collagen (1 mg/ml) and either sham exposed (A) or exposed to 1-MHz USWFs at pressure amplitudes of 0.1 (B) or 0.2 MPa (C). Samples were cultured for 10 days and then stained with MTT. Representative microscopy images are shown. Images are representative of three to four separate gels fabricated in at least three independent experiments. Scare bar: 250 µm. (D, E) Microvessel width (D) and density (E) were determined as described in the legend to Fig. 6. Data are presented as mean±s.e.m. of at least three gels fabricated on independent experimental days with three images obtained per gel. *, Significantly different from other groups (ANOVA, *P<0.05). The horizontal bar in E represents statistical significance (Student's t-test, P<0.05).

environments. Here, ultrasound technologies were employed for both directing the fabrication and imaging the structure of collagen hydrogel constructs that comprised endothelial cells patterned in 3D. Furthermore, integration of USWF patterning techniques and high-frequency ultrasound imaging tools enabled fabrication of 3D microvessel constructs with defined microvessel size and alignment. Ultrasound technologies provide unique advantages because they are non-invasive, non-destructive and can easily be incorporated into sterile environments required for cell culture. Further advances of these and other related ultrasound-based technologies holds promise for providing new methods to rapidly and non-invasively direct cell organization and fabricate vascularized tissues for microphysiological systems research and regenerative therapies.

MATERIALS AND METHODS

USWF apparatus

Unfocused, piezoceramic transducers with an acoustic frequency of 0.5, 1 or 2 MHz were fixed in the side of a plastic tank filled with degassed, deionized water (depicted in Fig. 1A). Characteristics of each transducer investigated are provided in Table S1. A waveform generator (Agilent 33220A, Santa Clara, CA), radio-frequency power amplifier (E&I, Rochester, NY) and an attenuator (Kay Electronics Corp., Lincoln Park, NJ) were used to drive the transducers. Ultrasound fields were calibrated at the beginning and end of each experiment by using either a membrane [Marconi bilaminar polyvinylidene fluoride (PVDF), Marconi Research Center, Chelmsford, UK] or a needle (ONDA Corporation, Sunnyvale, CA) hydrophone. Signals were measured by using a digital oscilloscope (Waverunner LT342, LeCroy Corp., Chestnut Ridge, NY). Transaxial beam patterns of each transducer at the exposure distance were measured by using a hydrophone; −6 dB beam widths were 1.0, 1.4 and 1.0 cm for sources at 0.5, 1 and 2 MHz, respectively.

Sample holders

Samples were contained in plastic cuvettes (1×1×3.4 cm, $l\times w\times h$). Parallel sides of each cuvette were removed and replaced with materials to minimize reflections (Fig. 1B). For samples prepared for high-frequency ultrasound imaging, one cuvette side was replaced with Saran wrap and the other side was replaced with a BioFlex silicone elastomer membrane (Flexcell International, Burlington, NC). For samples prepared for analysis of microvessel network morphology, both cuvette sides were replaced with BioFlex membranes lined with nylon or polypropylene mesh (McMaster-Carr, Aurora, CO). The mesh was pre-coated with collagen (250 µg/ml) to facilitate attachment of the cell-embedded collagen hydrogel to the cuvette walls and thus maintain the distance between initial locations of the planar cell bands during the 10-day culture period.

Cell culture and collagen gel preparation

Human umbilical vein endothelial cells (HUVECs, Lonza, Walkersville, MD) were used between passages four and eight. HUVECs were cultured in MCDB-131 (Gibco, Grand Island, NY) supplemented with 10% v/v fetal bovine serum (FBS, Hyclone, Logan, UT), 0.8% v/v ENDOGRO (VecTechnologies, Rensselaer, NY) and 2 mM L-Glutamine (GlutaMAX, Gibco). Adult human dermal microvascular endothelial cells (HMVEC-D, Lonza, Walkersville, MD) were used between passages three and eight. HMVEC-D were cultured in EGM-2MV (Lonza, Walkersville, MD). For HUVEC- or HMVEC-D-embedded collagen gels, medium was supplemented with 20 ng/ml phorbol 12-myristate 13-acetate (PMA, Sigma Aldrich, St Louis, MO) and penicillin–streptomycin (Gibco), and exchanged daily.

Neutralized type I collagen solutions were prepared as described previously (Garvin et al., 2011). Type I collagen (Corning, Bedford, MA), 2× concentrated Dulbecco's modified Eagle medium (DMEM, Gibco), and 1× concentrated DMEM (Gibco) were mixed on ice such that the final solutions had a concentration of 1 mg/ml collagen in 1× concentrated DMEM. Aliquots of DMEM were degassed prior to mixing to minimize gas bubbles.

Aliquots of HUVECs or HMVEC-D (1×10^6 cells/ml unless otherwise noted) were mixed with the collagen solution and immediately transferred into sample holders that had been positioned precisely at the exposure location of ultrasound field (Table S1). HUVEC samples were exposed to an USWF for 15 min using exposure parameters shown in Table S1. HMVEC-D samples were exposed to 1-MHz USWFs for 15 min using pressure

amplitudes of 0, 0.1 or 0.2 MPa. Following exposure, samples were either imaged immediately by using high-frequency ultrasound or cultured at 37°C and 5% CO_2 for 10 days. Sham samples were subjected to identical protocols as USWF-exposed samples but the sound was not activated.

High-frequency ultrasound imaging

High-frequency ultrasound imaging was utilized to visualize cell patterning throughout collagen hydrogels with volumes of 1×1×1 cm (Fig. 1C). High-frequency imaging techniques have been described previously (Mercado et al., 2014, 2015). Briefly, a pulser-receiver (5073PR, Olympus, Waltham, MA) generated a broadband pulse to excite a 38-MHz, focused PVDF transducer (PI50-2, Olympus, Waltham, MA) at a pulse repetition frequency (PRF) of 1 kHz. As reported previously (Mercado et al., 2014), the transducer had an aperture of 6.35 mm, focal length of 21 mm, −6 dB beam width of 170 µm, pulse length of 41 µm, depth of field of 4.7 mm and bandwidth of 13-47 MHz. The focus of the transducer was oriented in the center of the volume of each sample by using a three-axis positioning system. The center 6 mm of each sample was then scanned vertically at imaging locations separated by one beam width. Ultrasound backscattered RF signals were recorded with a digital oscilloscope (Waverunner 62Xi-A, LeCroy Corp., Chestnut Ridge, NY). At each scan location, 60 acquisitions were averaged to increase signal-to-noise ratios. Data from the oscilloscope were sent to a computer and compiled offline to generate backscatter (B-scan) images of the exposed samples (Mercado et al., 2014).

Post-processing of B-scan images was then performed to characterize cell patterning. The axial beam pattern of the 38-MHz transducer was measured and used to compensate for ultrasound beam diffraction. Illumination-flattening software was then used to compensate for ultrasound attenuation through the samples. Grayscale values of each pixel within each column of an image were then summed and plotted as a function of lateral distance. Three quantitative metrics were then extracted from these graphs to characterize the spatial patterning of cells (as depicted in Fig. 1C). First, the lateral distance between adjacent peaks and adjacent troughs was used to quantify the distance between adjacent cell bands. Second, the full width, half maximum value of each peak was used to quantify cell band width. Third, the difference in magnitudes of peaks and troughs (i.e. NAC) was used to quantify cell band density.

Analysis of microvessel network morphology

Sham and USWF-patterned samples were cultured for 10 days and then stained using thiazolyl Blue tetrazolium bromide (MTT, USB, Cleveland, OH), as described previously (Garvin et al., 2010; Mosmann, 1983). Phase-contrast images were obtained by using an Olympus IX70 microscope and digital camera (EXi Blue; QImaging). Microvessel width and alignment measurements were obtained by overlaying a grid (100 pixels by 100 pixels) on each image. Data were collected at grid intersections. To quantify vessel density, images were first converted to a binary format. A contrast-limited adaptive histogram equalization process was applied to each image in Fiji (ImageJ software; NIH) to reduce unevenly lighted areas; processed images were converted to a binary format using the Yen threshold algorithm such that viable, MTT-stained networks appeared black. Vessel density was then measured as the percentage of black pixels within the total image area.

In other experiments, samples were fixed for 1 h in 4% paraformaldehyde, processed using standard procedures and embedded in paraffin. Samples were serially sectioned (7 µm thick) perpendicular to the initial planar bands of cells and sections were stained with hematoxylin and eosin. Analyzed sections were obtained from at least 500 µm into the gel. Images were obtained using an Olympus BX60 microscope and digital camera (MicroPublisher 3.3; QImaging). ImageJ software was used to quantify lumen area on each of five sections collected from two collagen gels per exposure condition that had been obtained on separate days. Collagen gels were step-sectioned to ensure at least 150-µm intervals between measurements. At least 25 images were analyzed per section.

Immunostaining and confocal microscopy

HUVECs were patterned by using 1-MHz USWFs with pressure amplitudes of 0 (sham), 0.1, 0.2 and 0.3 MPa. Following a 10-day incubation at 37°C and 5% CO_2, gels were fixed with 4% paraformaldehyde, permeabilized with 0.5% Triton X-100, and blocked with 1% BSA, 10 mg/ml glycine and 0.05% Tween. Samples were incubated overnight at 4°C with a 1:100 dilution of rabbit anti-VE-cadherin polyclonal antibodies (#2158; Cell Signaling Technology, Danvers, MA) followed by Alexa-Fluor-594-conjugated goat anti-rabbit IgG secondary antibodies (Invitrogen, Carlsbad, CA). Cell nuclei were labeled with 60 nM 4′,6-diamidino-2-phenylindole (DAPI) dilactate (Invitrogen, Carlsbad, CA). Gels were examined by using an Olympus IX 70 microscope equipped with a Disk Scanning Unit (Olympus, Canter Valley, PA) and a 40× UApo/340 oil 0.90 NA objective (Olympus, Canter Valley, PA). Images were obtained at 5-µm intervals by using a SensiCam QE CCD camera (PCO-Tech Inc., Romulus MI) and *z*-stack images were projected using MicroManager software (version 1.4, San Francisco, CA).

Statistical analysis

Unless otherwise noted, all experiments were performed on at least three separate occasions. Single or duplicate gel samples were fabricated for each exposure condition during each independent experiment. Data are presented as mean±s.e.m. Statistical comparisons between conditions were performed by using a one-way analysis of variance (ANOVA) with Bonferroni post hoc tests using GraphPad Prism Version 4 software (La Jolla, CA). Differences between groups were considered significant for P-values <0.05.

Acknowledgements

The authors acknowledge the contributions of Sarah Wayson (University of Rochester, Rochester, NY) and Dr Maria Helguera (Rochester Institute of Technology, Rochester, NY) in image processing. D.C.H. and D.D. are co-senior authors.

Competing interests

D.D. and D.C.H. are named inventors on United States patent application PCT/US10/31281.

Author contributions

E.S.C. contributed to study conception, methodology, performing experiments, formal analysis, writing the manuscript and funding acquisition. D.D. and D.C.H. contributed to study conception, methodology, formal analysis, writing the manuscript, supervision, project administration and funding acquisition.

Funding

This work was supported, in part, by a grant from the National Institutes of Health [grant number: R01 EB018210], an American Heart Association (AHA) Pre-doctoral Fellowship [grant number: 15PRE25300000] and a grant to the University of Rochester School of Medicine and Dentistry from the Howard Hughes Medical Institute through the Med-into Grad Initiative [grant number: 56006775]. Deposited in PMC for release after 12 months.

Supplementary information

Supplementary information available online at
http://jcs.biologists.org/lookup/doi/10.1242/jcs.188151.supplemental

References

Bae, H., Puranik, A. S., Gauvin, R., Edalat, F., Carrillo-Conde, B., Peppas, N. A. and Khademhosseini, A. (2012). Building vascular networks. *Sci. Transl. Med.* **4**, 160ps23.

Bazou, D., Kuznetsova, L. A. and Coakley, W. T. (2005). Physical enviroment of 2-D animal cell aggregates formed in a short pathlength ultrasound standing wave trap. *Ultrasound Med. Biol.* **31**, 423-430.

Blinder, Y. J., Freiman, A., Raindel, N., Mooney, D. J. and Levenberg, S. (2015). Vasculogenic dynamics in 3D engineered tissue constructs. *Sci. Rep.* **5**, 17840.

Bouyer, C., Chen, P., Güven, S., Demirtaş, T. T., Nieland, T. J. F., Padilla, F. and Demirci, U. (2016). A bio-acoustic levitational (BAL) assembly method for engineering of multilayered, 3D brain-like constructs, using human embryonic stem cell derived neuro-progenitors. *Adv. Mater.* **28**, 161-167.

Corada, M., Mariotti, M., Thurston, G., Smith, K., Kunkel, R., Brockhaus, M., Lampugnani, M. G., Martin-Padura, I., Stoppacciaro, A., Ruco, L. et al. (1999). Vascular endothelial-cadherin is an important determinant of microvascular integrity in vivo. *Proc. Natl. Acad. Sci. USA* **96**, 9815-9820.

Dalecki, D. (2004). Mechanical bioeffects of ultrasound. *Annu. Rev. Biomed. Eng.* **6**, 229-248.

Dalecki, D. and Hocking, D. C. (2015). Ultrasound technologies for biomaterials fabrication and imaging. *Ann. Biomed. Eng.* **43**, 747-761.

Dalecki, D., Comeau, E. S., Raeman, C. H., Child, S. Z., Hobbs, L. and Hocking, D. C. (2015). Guiding tissue regeneration with ultrasound in vitro and in vivo. *Proc. SPIE* **9467**, 94670F1-94670F7.

Dalecki, D., Mercado, K. P. and Hocking, D. C. (2016). Quantitative ultrasound for nondestructive characterization of engineered tissues and biomaterials. *Ann. Biomed. Eng.* **44**, 636-648.

Garvin, K. A., Hocking, D. C. and Dalecki, D. (2010). Controlling the spatial organization of cells and extracellular matrix proteins in engineered tissues using ultrasound standing wave fields. *Ultrasound Med. Biol.* **36**, 1919-1932.

Garvin, K. A., Dalecki, D. and Hocking, D. C. (2011). Vascularization of three-dimensional collagen hydrogels using ultrasound standing wave fields. *Ultrasound Med. Biol.* **37**, 1853-1864.

Garvin, K. A., Dalecki, D., Yousefhussien, M., Helguera, M. and Hocking, D. C. (2013). Spatial patterning of endothelial cells and vascular network formation using ultrasound standing wave fields. *J. Acoust. Soc. Am.* **134**, 1483-1490.

Gol'dberg, Z. (1971). Radiation forces acting on a particle in a sound field. In *High Intensity Ultrasonic Fields* (ed. L. Rozenberg), pp. 109-117. New York: Plenum Press.

Gor'kov, L. (1962). On the forces acting on a small particle in an acoustical filed in an ideal fluid. *Sov. Phy. Dokl.* **6**, 773-775.

Gould, R. K. and Coakley, W. T. (1974). The effects of acoustic forces on small particles in suspension. In *Finite Amplitude Wave Effects in Fluids: Proceedings of the 1973 Symposium* (ed. L. Bjorno), pp. 252-257. Guildford: IPC Science and Technology Press LTD.

Hitchcock, T. and Niklason, L. (2008). Lymphatic tissue engineering: progress and prospects. *Ann. N. Y. Acad. Sci.* **1131**, 44-49.

Lin, R.-Z. and Chang, H.-Y. (2008). Recent advances in three-dimensional multicellular spheroid culture for biomedical research. *Biotechnol. J.* **3**, 1172-1184.

Liu, J., Kuznetsova, L. A., Edwards, G. O., Xu, J., Ma, M., Purcell, W. M., Jackson, S. K. and Coakley, W. T. (2007). Functional three-dimensional HepG2 aggregate cultures generated from an ultrasound trap: comparison with HepG2 spheroids. *J. Cell. Biochem.* **102**, 1180-1189.

Mercado, K. P., Helguera, M., Hocking, D. C. and Dalecki, D. (2014). Estimating cell concentration in three-dimensional engineered tissues using high frequency quantitative ultrasound. *Ann. Biomed. Eng.* **42**, 1292-1304.

Mercado, K. P., Helguera, M., Hocking, D. C. and Dalecki, D. (2015). Noninvasive quantitative imaging of collagen microstructure in three-dimensional hydrogels using high-frequency ultrasound. *Tissue. Eng. Part C Methods* **21**, 671-682.

Mosmann, T. (1983). Rapid colorimetric assay for cellular growth and survival: application to proliferation and cytotoxicity assays. *J. Immunol. Methods* **65**, 55-63.

Staton, C. A., Reed, M. W. R. and Brown, N. J. (2009). A critical analysis of current in vitro and in vivo angiogenesis assays. *Int. J. Exp. Pathol.* **90**, 195-221.